Numerical simulations of a PVC cable fire on long cable-trays in a mechanically ventilated large scale facility*

Hay, W., Seguillon, J. and Boyer, G.

IRSN, Centre de Cadarache, B.P. 3, 13115, St-Paul-lez-Durance Cedex, France

ARTICLE INFO

Keywords:
Computational Fluid Dynamics
Cable-tray fire
FLASH-CAT
PRISME-3
CALIF^{3}S-Isis

ABSTRACT

Electrical cable-tray fires pose a known safety risk at nuclear power plants. As part of the OECD funded PRISME-3 experimental programme, IRSN aims to improve understanding of cable-tray fires in confined and ventilated environments. In this study, a PVC cable fire in horizontally stacked long cable-trays is simulated using the CALIF^{3}S-Isis CFD code. A FLASH-CAT approach approximates the heat release rate profile and allows for flame front tracking, a potentially important characteristic for fires involving long cable-trays. A further equivalent simulation without flame-front tracking is also carried out, injecting the same total mass but this time over the combined upper surface areas of the cable trays. Comparisons suggest that the flame-front tracking approach reduces the maximum error seen in the CFD predictions of temperatures in the near-fire zone. A similar result is found for gas product concentrations. However, a quantitative analysis suggests that, in its current state, the implemented FLASH-CAT approach requires further improvements if it is to realise its potential to reduce errors in long cable-tray fire simulations. Suggested improvements relate to the mass loss rate per unit area profile implemented in the FLASH-CAT approach to improve the predictive capabilities of flame-front tracking methods.

1. Introduction

Since the 1980s, almost half of the 550 fire events recorded on Nuclear Power Plants (NPPs) have been caused by electrical equipment failure [1]. Such electrical failures can lead to ignition of the plastic materials which make up electrical cables. As several hundred kilometers of electrical cables can be found in NPPs, they pose a significant fire hazard, with one example of a serious cable fire occurring at the Browns Ferry NPP in 1975 [2]. Electrical cables are often grouped together and installed in trays, hereon fires associated with such a configuration are referred to simply as *cable-tray fires*.

In cable-trays, fire spreads both horizontally through the tray, and vertically through the stack, consuming the combustible material until flammability conditions are removed. Understanding this propagation and extinction phenomena is essential to the correct modelling of risk of fire scenarios on NPPs. In this context, efforts have been made to increase knowledge of such fires and to develop experimental databases, enabling numerical tools to better predict their potential consequences.

Early experimental campaigns were aimed at quantifying the combustion behaviour of cable-tray fires in free burning, open-atmospheres for a selection of cable-types [3]. It was later established that Heat Release Rate (HRR) data from both large and small scale tests are required to understand spread in cable-tray fires [4]. With this in mind, different cable types underwent testing at bench- and real-scale with the aim of developing correlations between the two [5].

Progress was made when focus was shifted to providing information on difficult-to-obtain data such as HRR and, significantly, flame spread rates [6]. Later, experimental data was provided in a series of experiments known as the CHRISTIFIRE campaign [7]. This data confirmed and validated the calculation methods outlined in the original NUREG/6850 report [6] and led to the development of a model for upward fire spread in horizontal tray configurations called FLASH-CAT (Flame Spread over Horizontal Cable Trays). The model takes input parameters including the combustible mass per unit area, effective heat of combustion and heat release rates per unit area and outputs a local fire duration allowing for dynamic predictions of flame spread and extinction. Recommended values for the aforementioned parameters were provided for both thermoset and thermoplastic cable-types and the semi-empirical model was shown to provide conservative HRR predictions [7].

Later, the predictive capabilities of the FLASH-CAT approach were further developed [8]. Improvements included the horizontal flame propagation velocities being calculated based on Quintiere's correlation [9], using local temperature and oxygen measurements. It was then observed that a supporting back-wall for the cable-trays could accelerate fire spread [10]. In the latter reference, video analysis was also used to provide improvements to the NUREG/7010 recommended propagation velocities.

The FLASH-CAT approach can be predictive, where propagation is calculated from models relying on local measurements, or non-predictive, where propagation is set by input parameters found from experimental measurements. In both cases, integrating a model based on the FLASH-CAT approach into 3D numerical software, allows the flame front

*This work was completed as part of the PRISME programme, an international research programme carried out by IRSN under the aegis of the OECD.

william.hay@irsn.fr (H. W.)
ORCID(s): 0000-0002-3151-9003 (H. W.)

to be tracked and can theoretically improve the accuracy of CFD predictions.

An alternative approach to CFD modelling of cable-tray fires with propagation is to arbitrarily split the trays into combustible material and air slots to simulate a loose arrangement [11]. Thermal properties, ignition temperatures and heat release rates for the combustible material then originate from cone calorimetry. It has been found, however, that modifying the heat release rate profile from cone calorimetry is necessary to reproduce the full-scale results.

In this study, a model based on the FLASH-CAT approach is integrated in the CALIF^{3}S-Isis CFD code. Dedicated to fire simulations, the code has been extensively validated in the past [12, 13] and applied to similar studies involving fires under confined and mechanically-ventilated conditions [14, 15, 16]. The propagation of the fire is captured using a FLASH-CAT approach unique to CALIF^{3}S-Isis. Parameters determining the propagation can either be predicted via models, or supplied by the user *a priori* from experimental measurements, a method also adopted in Ref. [17]. The latter approach is adopted here and the parameters defining the fire propagation are taken directly from the experimental measurements of Ref. [18].

A previous study used the same implemented FLASH-CAT approach in CALIF^{3}S-Isis to simulate fire experiments carried out by the Institut de Radioprotection et de Sûreté Nucléaire (IRSN) in the framework of the Cable Fire Spread (CFS) campaign of the OECD PRISME-2 project [19]. A five tray configuration of halogen-free flame retardant cables was studied and the HRRs were well reproduced in the simulations when propagation parameters originated from experimental video analysis. Furthermore, the predictions of gas temperatures in the fire room were in good agreement with the experimental results.

The fire scenario studied here is part of the Cable Fire Propagation (CFP) test campaign carried out in the framework of the OECD PRISME-3 project. In this campaign, the propagation of cable fires on long cable-trays was studied in a series of experiments in confined and ventilated environments [18]. It differs from the scenario considered in the previous numerical study [19], in that the fire room is a corridor connected to three other non-communicating rooms, the cable-type is polyvinyl chloride (PVC) and the tray stack involves three, longer, cable trays which are ignited from one end and propagate towards the other. In long cable-trays, knowledge of the flame front location is particularly important.

Often, experimental data does not exist for flame propagation over cable-trays. Hence, the approach without flame-front tracking is often adopted whereby an equivalent MLR profile is injected over the total of the burning surface area of the cable-trays. In this study, we carry out a second simulation adopting a similar approach for comparative purposes. The aim of this study is then to compare predictions of simulations with and without flame-front tracking to see the influence on the temporal evaluations of temperatures above the cable-trays, local oxygen depletion and heat fluxes opposite the fire.

In Section 2, the experiment is described, in Section 3, the adopted FLASH-CAT approach is provided in more detail. In Section 4, the simulation and numerical set-up are discussed. In Section 5, we discuss the results and finally, in Section 6, conclusions are drawn.

2. Description of the experiment

The CFP corridor experimental campaign involved a series of fire experiments under contained and ventilated conditions. In each test, the fire source involved three horizontal ladder-type cable trays with widths of 0.45 m, stacked one upon the other with a vertical spacing, h, of 0.3 m. The 6 m long trays were ignited from one end, with the fire then propagating towards the other. The aforementioned tray parameters are provided in Table 1. The trays themselves were set against a back-wall in order to thermally protect the concrete wall behind. The back-wall-mounted stack was then located in the corridor of the DIVA facility, discussed further in Section 2.1, with the corridor connected to three non-communicating adjacent rooms.

2.1. DIVA facility

The fire source was located in the DIVA facility, shown in Fig. 1, which is made up of two levels. The lower level contains three rooms each connected to a corridor, whereas the upper level is a single room which plays no role in the experimental campaign. The three lower rooms (R1, R2 and R3) are of equal size, 6 m × 5 m × 4 m, and the corridor measures 15.6 m × 2.5 m × 4 m.

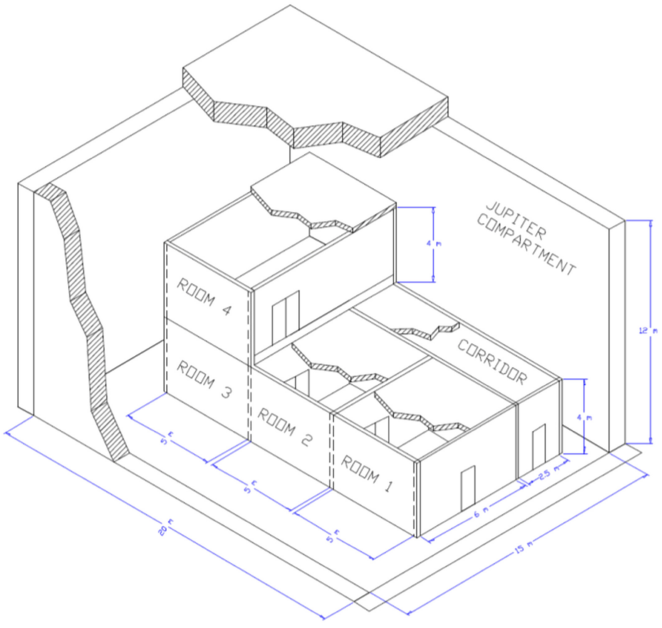

Figure 1: DIVA facility

Table 1
Tray and cable parameters from the PVC cable-tray fire experiment of the CFP corridor campaign.

Tray parameters			Cable parameters	
No. trays	Area (m^2)	Spacing (m)	No. cables	Type
3	6 × 0.45	0.30	21	PVC

2.2. PVC cable-tray fire experiment

In the PVC cable-tray fire experiment, each tray was filled with 21 PVC cables 6 m in length, loosely arranged to avoid over-packing. The aforementioned cable parameters are provided in Table 1. The loose arrangement of the PVC cables, visible in Fig. 2, promotes vertical propagation between the cable-trays. The PVC cables used in the experiment are 28 mm in diameter, containing 5 x 25 mm^2 power cables surrounded by several halogenated polymer layers of sheath, filler and insulation.

Figure 2: Cable-tray installation in the corridor of the DIVA facility. In this photo, we note the loose arrangement of the 21 PVC cables per tray.

The cables were ignited at one end by a propane sand burner of dimensions 0.3 x 0.3 m^2, located 0.2 m below the lowest tray. The 80 kW burner corresponds to a propane mass flow rate of 1.74 g/s. As the fire propagated and combustion became self-sufficient, the burner was stopped when the fire was observed to have progressed horizontally across 50% of one of the cable-trays, that is when 3 m of cable on at least one tray was burnt or was burning. For the PVC cable-tray experiment, this corresponded to 20 minutes of burning time. The experiment itself was considered over when no further mass loss occurred. The mass being continuously measured during the experiment by four electronic scales placed underneath the assembly of the frame, trays and burner.

2.3. Ventilation network

Prior to ignition, the ventilation network of the DIVA facility established admission flow rates of ∼1500 m^3/h into each room and the corridor, and extraction flow rates of ∼3000 m^3/h from R3 and the corridor only. A nodal representation of the ventilation network and the corresponding measured values for pressures and flow rates are provided in Fig. 3 and Table 2. The aforementioned flow rates then ensure a room renewal rate of 12.9 h^{-1}.

Table 2
Ventilation parameters prior to ignition in the PVC cable-tray fire experiment. The measurements of pressure, $P_{r,b}$ (Pa), flow rates, $\dot{V}_{r,b}$ (m^3/h), and resistances, $R_{r,b}$ (Pa s/m^3) where r = room and b = branch, are averages representing steady state conditions.

$P_{C,adm}$	$P_{1,adm}$	$P_{2,adm}$	$P_{3,adm}$	$P_{C,ext}$	$P_{3,ext}$
101868	101843	101853	101870	100847	100984
$\dot{V}_{C,adm}$	$\dot{V}_{1,adm}$	$\dot{V}_{2,adm}$	$\dot{V}_{3,adm}$	$\dot{V}_{C,ext}$	$\dot{V}_{3,ext}$
1540	1510	1530	1550	3100	3060
$R_{C,adm}$	$R_{1,adm}$	$R_{2,adm}$	$R_{3,adm}$	$R_{C,ext}$	$R_{3,ext}$
2867	2866	2830	2848	433	286

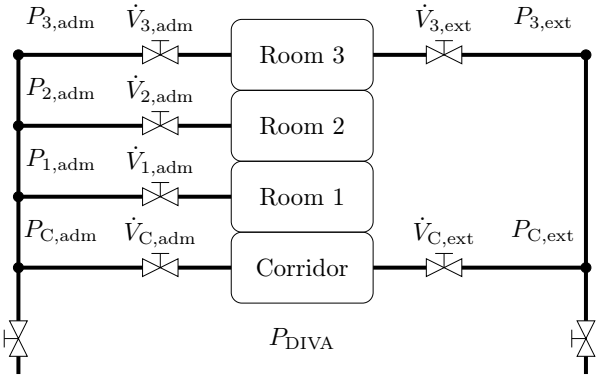

Figure 3: Nodal ventilation network for the considered experiment in the DIVA facility. The initial pressure in the DIVA facility, P_{DIVA} $(t = 0)$, was measured at 101232 Pa.

3. FLASH-CAT approach

In this section, we provide an overview of the implemented FLASH-CAT approach specific to CALIF^{3}S-Isis. The aim is to provide an accurate as possible estimation of the HRR evolution for a cable-tray fire scenario, using time-averaged quantities and material parameters. The model assumes that fire spreads both horizontally and vertically. In this study, the fire propagates from one end of the cable-tray to the other in the horizontal direction indicated by the red arrow in Fig. 4. Further, combustion is assumed to begin in the first tray above the burner, with the initial burning length in the first tray, $L_1(t = 0)$, equal to the burner width, 0.30 m. The instantaneous tray burning lengths, $L_i(t)$ where $i = 1, 2, 3$ is the tray index, are dynamic quantities representing the distance between the flame and extinction fronts, i.e. the

tray combustion zone, which of course evolves as the fire propagates.

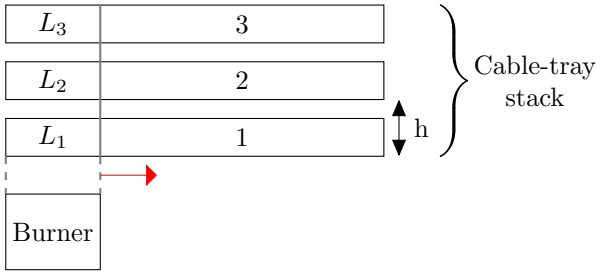

Figure 4: FLASH-CAT configuration for the stack of three cable trays. In this figure, $h = 0.3$ m, is the tray spacing and $L_i(t)$ is the instantaneous tray burning length with $i = 1, 2, 3$ as the tray index. The initial burning length of the first tray $L_1(t = 0)$ is equal to the burner width, or 0.30 m and the red arrow shows the direction of horizontal propagation.

Once ignited, the local fire duration, τ_f (s), is found from material parameters according to the following relation [7],

$$\tau_f = \frac{6m''_c}{5\dot{m}''_{avg}}, \tag{1}$$

where m''_c (kg/m^2) and $\dot{m}''_{avg}$ (kg/m^{2}s) are the combustible mass per unit area and average mass loss rate per unit area (MLRPUA), respectively.

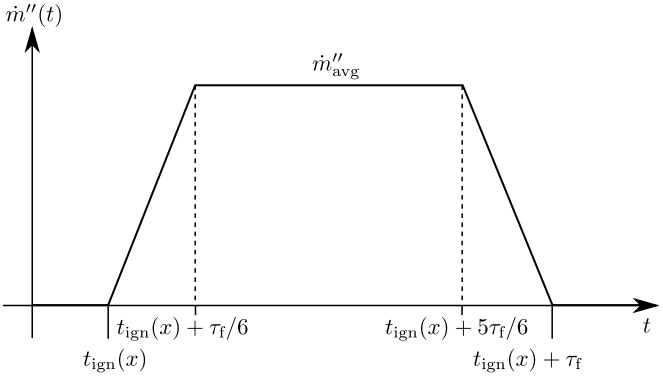

Figure 5: FLASH-CAT MLRPUA profile for an ignited zone on the cable tray. In this figure, $\dot{m}''_{avg}$ is the average MLRPUA and $t_{ign,i}(x)$ is the ignition time of the x-coordinate (cell face) of ith tray and τ_f is the local fire duration.

Further, the implemented FLASH-CAT approach requires propagation parameters in order to define the fire spread. These include the horizontal propagation velocities, v_i (mm/s), and the vertical propagation times, t_i (s). In the following paragraphs, we elaborate on the four FLASH-CAT input parameters mentioned above.

We begin with the combustible mass per unit area. In cable-tray combustion, the pyrolysing surface area is as difficult to measure experimentally as it is to model in a CFD simulation. As such, a simplified approach is adopted here, whereby m''_c is found by dividing the total mass burnt in the experiment, M_{tot}, by the available burning area in the simulation. In this study, pyrolysis occurs at the upper surface of the trays only. Therefore, the available burning area, A_{tot}, corresponds to the combined area of the upper surface of the three cable trays,

$$A_{tot} = 3 \times 0.45 \times 6 = 8.1\,\text{m}^2\,. \tag{2}$$

The total mass burnt during the experiment was measured at 121kg and we find $m''_c = 14.9\text{kg/m}^2$. A similar approach has been adopted in previous studies [19].

Next, we find the MLRPUA from the following relation,

$$\dot{m}''_{avg} = \frac{\dot{q}''_{avg}}{\Delta H_c}, \tag{3}$$

where $\dot{q}''_{avg}$ (kW/m^2) is the heat release rate per unit area and ΔH_c (MJ/kg) is the effective heat of combustion. The latter quantity is found from the experimental values of total heat release (THR) and total mass burnt as follows,

$$\Delta H_c = \frac{\text{THR}}{M_{tot}}\,.$$

Next, $\dot{q}''$ is found by from a time-average of the ratio of the experimentally measured HRR and the dynamic burning area,

$$\dot{q}''_{avg} = \left\langle \dot{q}''(t) \right\rangle_{\Delta t} \text{ where } \dot{q}''(t) = \frac{\dot{q}(t)}{L(t) \times W} \tag{4}$$

with $L(t)$ as the dynamic burning length and W the tray width, 0.45m, and where $< \cdots >_{\Delta t}$ is a time-averaging procedure over the fire duration, Δt. We note that post-processing video analysis of the experiments was used to measure $L(t)$ [18]. In finding $\dot{q}''_{avg} = 220$ kW/m^2 for the PVC cable-type we agree well with Ref. [7], which suggests 250 kW/m^2 for thermoplastic cables. We note, however, that the values for ΔH_c and $\dot{q}''_{avg}$ used here include the contribution of the propane burner which was in operation for $\sim 1/5^{th}$ of the duration of the experiment. Their values should therefore be used with caution for any future cable-tray fires involving PVC type cables.

The horizontal propagation velocities and the vertical propagation times are also taken from video analysis [18]. Moreover, the propagation angle used in previous FLASH-CAT models does not appear here as is set equal to zero. Results were shown to be insensitive to this parameter here and in a previous study [10]. The HRR and cumulative mass loss profiles predicted by the implemented FLASH-CAT approach using the parameters available in Table 3 are given in Figs. 6 and 7, respectively. As briefly discussed in the Introduction, two simulations are analysed in this paper. The first relies upon the FLASH-CAT approach developed above. The second, whose profiles are also plotted in Figs. 6 and 7, is an "equivalent" simulation with the same burnt mass ($M_{tot} = 121$kg) and total heat release ($\dot{V}_{tot} = 2580$MJ). The difference between the two simulations then lies in the fact that the FLASH-CAT approach allows for the fire propagation to be captured whereas the equivalent simulation does not.

Table 3
FLASH-CAT parameters. In this Table, M_{tot} is the total mass burnt, A_{tot} is the available burning area in the simulation, m''_c is the combustible mass per unit area, ΔH_c is the effective heat of combustion, $\dot{q}''_{avg}$ is the heat release rate per unit area, $\dot{m}''_{avg}$ is the mass loss rate per unit area, v_i are the horizontal propagation velocities and t_i (s) are the vertical propagation times, with $i = 1, 2, 3$ as the cable tray index. We note that the first tray is assumed alight at $t_1 = 0$ when combustion begins.

M_{tot} (kg)	A_{tot} (m^2)	m''_c (kg/m^2)	ΔH_c (MJ/kg)	$\dot{q}''_{avg}$ (kW/m^2)	$\dot{m}''_{avg}$ (kg/m^2s)	v_1 / v_2 / v_3 (mm/s)	t_1 / t_2 / t_3 (s)
121	8.1	14.9	21.3	220	0.011	1.70 / 1.97 / 2.33	0 / 66 / 144

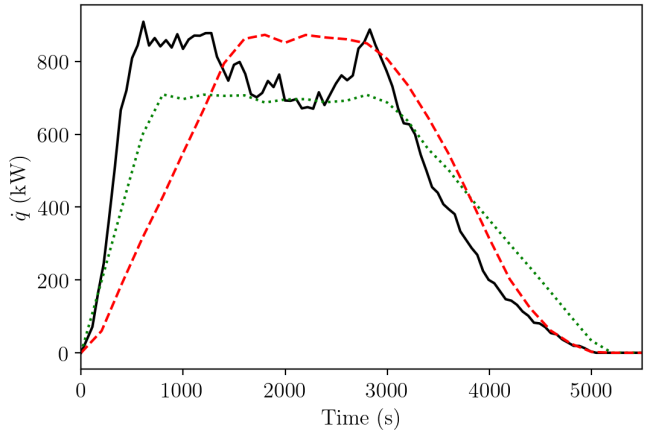

Figure 6: HRR plots. In this figure, the HRR profile is plotted for the experiment (——), the simulation adopting the FLASH-CAT approach (– – –) and the equivalent simulation without flame propagation (·····).

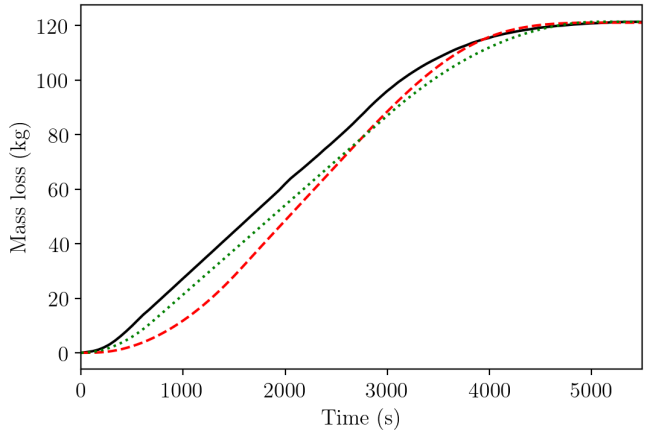

Figure 7: Cumulative mass loss plots. In this figure, the legend is the same as in Fig. 6. The cumulative mass loss at 5100s (fire duration) corresponds to the total mass burnt, in both simulations M_{tot} = 121kg.

4. Simulations

In this section, we present the governing equations and numerical set-up, including the mesh and the boundary and initial conditions for the simulations.

4.1. Governing equations

The CALIF^{3}S-Isis CFD software is a numerical field model dedicated to fire simulations conducted in confined and ventilated compartments. The code itself relies upon the low-Mach number approximation of the Navier-Stokes equations as buoyant fires, such as that investigated in this study, involve low-speed flows with significant variations in temperature. In this study, turbulence modelling is implemented using the standard two-equation RANS k-ε model and the reaction mechanism is reduced to a one-step reaction in which an equivalent fuel, representing the PVC cables, reacts with oxygen to produce products. Hereon, the turbulent combustion process is assumed to be mixing-controlled and is modelled using the Eddy-Dissipation Concept (EDC) approach.

The governing equations for the problem in hand are then the low-Mach-number approximation of the compressible Navier-Stokes equations, plus conservation equations for the total enthalpy h, the mixture fraction, z, and the fuel species, Y_f, which we expand upon in this section. The Favre-averaged [20] Navier-Stokes equations solve for mean fields and the full system reads as,

$$\frac{\partial \overline{\rho}}{\partial t} + \nabla \cdot (\overline{\rho}\widetilde{\mathbf{v}}) = 0\,, \tag{5}$$

$$\frac{\partial}{\partial t}(\overline{\rho}\widetilde{\mathbf{v}}) + \nabla \cdot (\overline{\rho}\widetilde{\mathbf{v}} \otimes \widetilde{\mathbf{v}}) = -\boldsymbol{\nabla}\overline{p'} + \nabla \cdot \left(2\mu_e \overline{\mathbf{S}}\right) + (\overline{\rho} - \rho_0)\mathbf{g}\,, \tag{6}$$

with $\overline{\mathbf{S}}$, the mean rate-of-strain tensor, defined as follows

$$\overline{\mathbf{S}} = \frac{1}{2}\left(\boldsymbol{\nabla}\widetilde{\mathbf{v}} + \boldsymbol{\nabla}^t\widetilde{\mathbf{v}}\right)\,. \tag{7}$$

In the above equations, $\overline{\rho}$ is the Reynolds-averaged density and $\widetilde{\mathbf{v}}$ is the Favre-averaged velocity. In low-Mach-number flows, the total pressure $\bar{P}$ is expressed as the sum of a thermodynamic part $\overline{P_{th}}$, a hydrodynamic part $\overline{p}$ and a hydrostatic part $\rho_0 \mathbf{g}z$. In Equation (6), the modified pressure $\overline{p'}$ relates to the hydrodynamic pressure as follows,

$$\overline{p'} = \overline{p} + \frac{2}{3}\left(\mu_e \nabla \cdot \widetilde{\mathbf{v}} + \overline{\rho}k\right)\,. \tag{8}$$

In the case studied here of a confined domain connected to a ventilation network, the thermodynamic pressure $\overline{P_{th}}$ is

found from the mass balance,

$$\frac{d}{dt}\int_{\Omega}\frac{\overline{P_{\rm th}}(t)W}{\mathcal{R}\widetilde{T}}+\sum_i \dot{m}_i \;=\; 0\,, \tag{9}$$

where $\sum_i \dot{m}_i$ is the sum of the mass flow rates for each branch connected to the ventilation network of the DIVA facility.

Then, the conservation equation for the Favre-averaged total enthalpy, $\widetilde{h}$ is expressed as,

$$\frac{\partial}{\partial t}(\overline{\rho}\widetilde{h})+\nabla\cdot(\overline{\rho}\widetilde{\mathbf{v}}\widetilde{h}) \;=\; \frac{d\overline{P_{\rm th}}}{dt}+\nabla\cdot\left(\overline{\rho}\alpha_e\boldsymbol{\nabla}\widetilde{h}-\widetilde{\boldsymbol{q}}_r\right) \tag{10}$$

$\widetilde{h}$ is defined as $\widetilde{h}=c_p\Delta\widetilde{T}+\widetilde{Y}_F\Delta H_c$, where $\Delta H_{\rm c}$ has been defined in Table 3.

4.1.1. Treatment of thermal radiation

The radiation source term, $\widetilde{\boldsymbol{q}}_r$, is computed via the resolution of the Radiative Transfer Equation written for a gray and non-diffusive media. It is integrated according to the Finite Volume Method [21], wherein the total set of admissible directions of propagation is discretised in a finite set of control angles characterised by the angular coordinates of its direction. The medium radiative abosrption includes the contribution of the main combustion products CO_2 and H_2O using the Weighted Sum of Grey Gases Model (WSGGM) [22], and of the soot. The soot absorption coefficient is then related to the soot volume fraction and scattering effect is neglected, according to the Mie theory [23].

4.1.2. Treatment of turbulence

In Equation (6), the standard k-ε RANS turbulent-viscosity model is used with the Boussinesq approximation for the closure of the Reynolds stresses. This introduces an effective viscosity, $\mu_e = \mu+\mu_t$, where μ_t is the turbulent viscosity expressed as

$$\mu_t \;=\; 0.09\,\overline{\rho}\frac{k^2}{\varepsilon}\,. \tag{11}$$

In Equation (11), k is the turbulent kinetic energy and ε is the turbulence dissipation rate. Finally, in Equation (10), α_e is the effective thermal diffusivity expressed as a function of μ , μ_t, the Prandtl number, $\mathcal{P}r$, and the turbulent Prandtl number, $\mathcal{P}r_t$,

$$\overline{\rho}\alpha_e \;=\; \rho\alpha+\frac{\mu_t}{\mathcal{P}r_t} \;=\; \frac{\mu}{\mathcal{P}r}+\frac{\mu_t}{\mathcal{P}r_t}\,. \tag{12}$$

Two additional transport equations, for k and ε, then need to be solved for,

$$\begin{aligned}\frac{\partial}{\partial t}(\overline{\rho}k)+\nabla\cdot(\overline{\rho}k\widetilde{\mathbf{v}}) \;&=\; \nabla\cdot\left[\left(\mu+\frac{\mu_t}{\sigma_k}\right)\boldsymbol{\nabla}k\right]\\ &+P_k+G_k-\overline{\rho}\varepsilon\,,\end{aligned} \tag{13}$$

and

$$\begin{aligned}\frac{\partial}{\partial t}(\overline{\rho}\varepsilon)+\nabla\cdot(\overline{\rho}\varepsilon\widetilde{\mathbf{v}}) \;&=\; \nabla\cdot\left[\left(\mu+\frac{\mu_t}{\sigma_\varepsilon}\right)\boldsymbol{\nabla}\varepsilon\right]\\ &+\frac{\varepsilon}{k}\left(C_{\varepsilon_1}P_k+C_{\varepsilon_1}(1-R_f)G_\varepsilon-C_{\varepsilon_2}\overline{\rho}\varepsilon\right)\,,\end{aligned} \tag{14}$$

where σ_k and σ_ε are the turbulent Prandtl numbers for k and ε, here set to 1 and 1.3, respectively. The Richardson number, $R_f = 0.3$, and C_{ε_1} and C_{ε_2} are model constants equal to 1.44 and 1.92, respectively. Also, P_k represents the production of turbulence kinetic energy due to the mean velocity gradients and G_k is the production of turbulence kinetic energy due to buoyancy, here modeled using the Generalised Gradient Diffusion Hypothesis (GGDH) as follows,

$$G_k \;=\; -\frac{3\mu_t}{\overline{\rho}^2 k\sigma_g}\left(\boldsymbol{\nabla}\widetilde{\mathbf{v}}\cdot\boldsymbol{\nabla}\overline{\rho}\right)\cdot\rho_0\mathbf{g}\,, \tag{15}$$

$$G_\varepsilon \;=\; \max(G_k,0)\,. \tag{16}$$

4.1.3. Chemistry and turbulent combustion modelling

As stated, we consider a single-step irreversible reaction of a fuel, F, reacting with an oxidizer, O, to produce products, P_k, summarized as follows,

$$\nu_{\rm F}F+\nu_O O\longrightarrow\;\sum\nu_{P_k}P_k\,, \tag{17}$$

where $\nu_{\rm F}$, ν_O and ν_{P_k} are the molar stoichiometric coefficients for the fuel, oxidizer and products, respectively. One can also define s_O and s_{P_k} as the associated mass stoichiometric coefficients using $s_O = \nu_O W_O/\nu_F W_F$ and $s_{P_k} = \nu_{P_k}W_{P_k}/\nu_F W_F$, where W_O, W_F and W_{P_k} are the molecular masses of oxygen, fuel and the products, respectively. In practise, for the PVC cable-type, the assumed equivalent fuel is C_2H_3Cl ($W_F = 62.5$g/mol) and the reaction scheme is given by,

$$\begin{aligned}&\nu_{\rm F}\,C_2H_3Cl+\nu_{O_2}\,O_2\longrightarrow\\ &\nu_{CO_2}\,CO_2+\nu_{H_2O}\,H_2O+\nu_{HCl}\,HCl+\nu_C\,C^{(s)}+\nu_{CO}\,CO\,,\end{aligned} \tag{18}$$

where $\nu_C = 0.21$ and $\nu_{CO} = 0.11$, are calculated from the experimentally measured mass yields, $s_C = 38$ and $s_{CO} = 52$ (mg/g). The remaining molar stoichiometric coefficients are then found as,

$$\begin{aligned}\nu_{\rm F} \;&=\; 1,\quad \nu_{H_2O} \;=\; 1,\quad \nu_{HCl} \;=\; 1\,,\\ \nu_{O_2} \;&=\; 2.5-\nu_C-\frac{\nu_{CO}}{2}\,,\\ \nu_{CO_2} \;&=\; 2.0-\nu_C-\nu_{CO}\,.\end{aligned}$$

In the original Eddy Dissipation Concept (EDC) model [24], only two variables are transported, namely the mean fuel mass fraction, $\widetilde{Y}_F$, and the mean mixture fraction $\widetilde{z}$ such as,

$$\widetilde{z} \;=\; \frac{\widetilde{Y}_F+s_O(Y_O^o-\widetilde{Y}_O)}{Y_F^f+s_O Y_O^o} \;=\; \frac{\widetilde{Y}_F+\widetilde{Y}_{P_k}/s_{P_k}}{Y_F^f}, \tag{19}$$

where Y_F^f and Y_O^o denote the fuel mass concentration in fuel stream and the oxidizer mass concentration in oxidizer

stream, respectively. The transport equation for the fuel mass fraction,

$$\frac{\partial}{\partial t}(\overline{\rho}\,\widetilde{Y}_F) + \nabla\cdot(\overline{\rho}\,\widetilde{\mathbf{v}}\,\widetilde{Y}_F) \;=\; \nabla\cdot\left(\overline{\rho}D_e\boldsymbol{\nabla}\widetilde{Y}_F\right) + \overline{\dot{\omega}}_F\,. \quad (20)$$

includes a combustion source term $\overline{\dot{\omega}}_F$ expressed as

$$\overline{\dot{\omega}}_F \;=\; -C_{\mathrm{edc}}\,\overline{\rho}\frac{\varepsilon}{k}\min\left(\widetilde{Y}_F, \frac{\widetilde{Y}_O}{s_O}\right), \quad (21)$$

with the model constant $C_{\mathrm{edc}} = 4$, whereas the transport equation for the mixture fraction,

$$\frac{\partial}{\partial t}(\overline{\rho}\,\widetilde{z}) + \nabla\cdot(\overline{\rho}\,\widetilde{\mathbf{v}}\,\widetilde{z}) \;=\; \nabla\cdot\left(\overline{\rho}D_e\boldsymbol{\nabla}\widetilde{z}\right) \quad (22)$$

is homogeneous. In Equations (20) and (22), D_e is the effective diffusivity expressed as a function of μ, μ_t , the Schmidt number, Sc, and the turbulent Schmidt number, Sc_t,

$$\overline{\rho}D_e \;=\; \rho D + \frac{\mu_t}{Sc_t} \;=\; \frac{\mu}{Sc} + \frac{\mu_t}{Sc_t}\,. \quad (23)$$

Once these equations are resolved, the remaining reactive species are deduced from Equation (19), whereas the neutral species is deduced from the unit sum over all the mass fractions.

Together, Equations (5) - (6), (10), (13) - (14), (20) and (22) represent the full system of equations to be solved. This system is then closed with an equation of state involving the thermodynamic pressure. In this study, the fluid is a gaseous mixture of chemical species, where the density is found from the ideal mixing rule,

$$\frac{1}{\overline{\rho}} \;=\; \sum_{k=1}^{N}\frac{\widetilde{Y}_k}{\overline{\rho}_k}\,, \quad (24)$$

where $\overline{\rho}_k$ stands for the density of the chemical species k, and is given by the ideal gas equation of state,

$$\overline{\rho}_k \;=\; \frac{\overline{P_{\mathrm{th}}}\,W_k}{\mathcal{R}\widetilde{T}}\,. \quad (25)$$

4.2. Numerical set-up

The computational domain is provided in Fig. 8. With respect to the boundary conditions, the admission and exhaustion lines consider the boundary to be connected to an external atmosphere not included in the computational domain but modelled by a resistance, R, representing a branch of the ventilation network. In this simulation, the following stationary Bernoulli equation is considered,

$$\overline{P_{\mathrm{th}}}(t) - P_{r,b} = \mathrm{sign}(\dot{m})R\frac{|\dot{m}|^{\alpha}}{\overline{\rho}^{\beta}}\,. \quad (26)$$

The thermodynamic pressure and the admission and exhaust mass flow rates are determined by coupling the Bernoulli equation above with the overall mass balance equation, Eq. 9. Prior to ignition, the mass flow rates and resistances used to establish a steady-state room renewal rate of 12.9 h^{-1} in the simulations are given in Table 2. These hydraulic resistances result in mass flow rates of 0.5 and 1.0 kg/s for the admission and extraction lines, respectively.

Table 4
Wall and ceiling material properties.

	ρ (kg/m³)	c_p (J/kg K)	λ (W/m K)
Concrete	2240	820	1.50
Calcium silicate	970	970	0.22
Insulation	360	840	0.09
Air	1	1000	0.04

In order to accurately calculate the heat transfer in the domain it is necessary to model the heat conduction, via Fourier's law, at solid boundaries. The walls and ceiling are concrete, with the vertical sidewalls being 0.30 m thick. For thermal protection, concrete panels (0.065 m) are added at all sidewalls, with further insulation (0.02 m) added in regions opposite the fire in the corridor. With regards to the ceiling, thermal protection is ensured by three layers of air (0.10 m), insulation panels (0.01 m) and calcium silicate, panels (0.0127 m). The material properties required to capture the heat transfer at solid boundaries are the density, ρ, the specific heat capacity, c_p, and the thermal conductivity, λ. All of which are provided in Table 4. We note here that the air thermal conductivity has been increased by a factor of two in order to take into account the convective heat transfer not modelled.

Pyrolysis from the cables is represented by a mass loss (or injection of fuel) at the upper surfaces of the cable-trays. The rate of injection depends on whether or not the FLASH-CAT approach is adopted. For the case utilising FLASH-CAT, the injection area evolves with time as the flame front propagates across the burning trays. On the other hand, for the "equivalent" simulation, the injection occurs over the entire 8.1m^2 available area. The temperature of the cable trays is initially set to the local gas temperature measured in the facility. However, during and following combustion, the temperature is set to the pyrolysis temperature of 330° C.

The initial conditions of the simulation are quiescent air at the ambient temperature and pressure of 20° C and 101232 Pa, respectively. The latter measurements being taken in the DIVA facility before the experiment began. The simulations are first run for ten seconds to initialize the ventilation network before combustion begins.

4.3. Discretisation parameters

The fluid domain shown in Fig. 8 is discretised into a numerical grid, shown from above in Fig. 9. The mesh is refined in areas of interest, that is in the corridor and in the combustion zone near the fire source. In this latter zone, refinement is in the vertical direction, in order to better capture the flame behaviour.

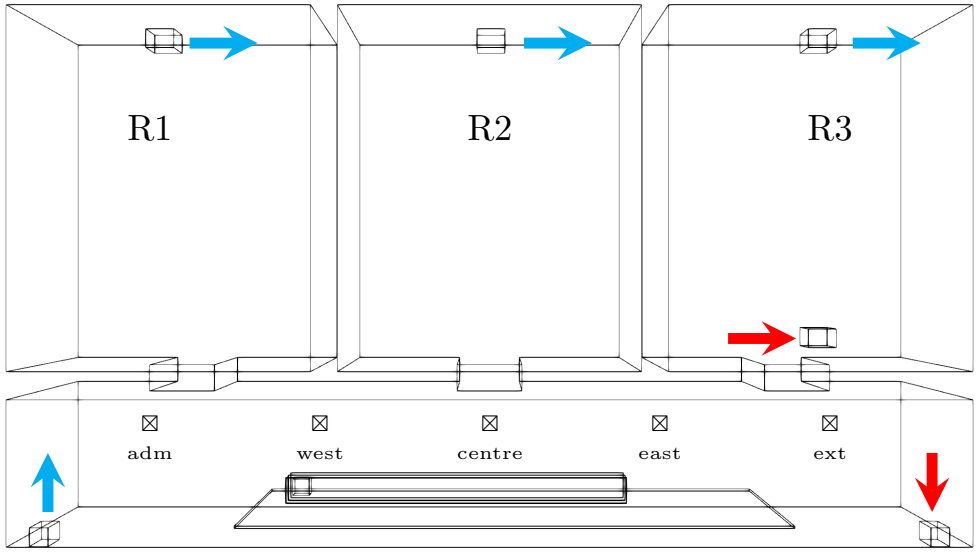

(a) Full domain viewed from above.

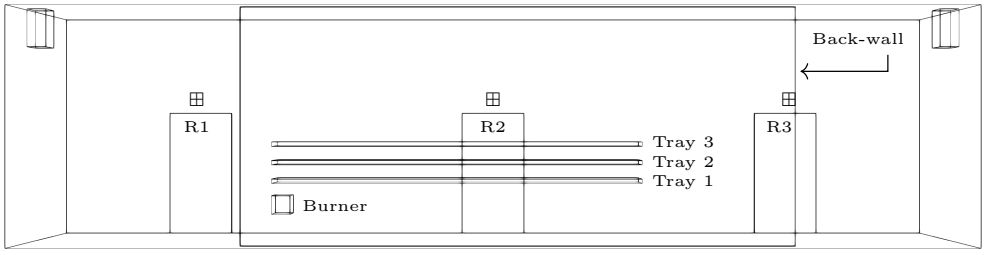

(b) Corridor viewed from behind.

Figure 8: Computational domain. In this figure, the arrows represent the ventilation lines; blue for admission and red for extraction. Viewed from above the corridor sits south of the three rooms. Here, the cable-trays are mounted on the backwall and the cable-tray is ignited on the admission-side (adm) and propagates towards the extraction-side (ext). Also visible in the corridor are the locations of the thermocouple trees and gas analysers, (⊠). The side-view shows the burner position, trays, back-wall and the location of the heat flux sensors above the doorways (⊞).

A mesh sensitivity analysis was performed on a coarse, intermediate and fine mesh, respectively made up of 0.5, 1.0 and 2.5 million cells, with reference cell sizes in the fire zone of 0.058 m, 0.045 m and 0.037 m, respectively. Predictions of temperatures, heat fluxes and concentrations between the intermediate and the fine mesh differed by an average of 1 and a maximum of 4%. The intermediate mesh was then used for all simulation results presented in this study. Table 5 describes the mesh on a per-room basis. We note that in the fire zone, the cell size corresponds to 10% of the integral length-scale, with this latter quantity equal to the tray width.

The partial differential equations (5) - (10), (13) - (14) and (22) - (20) are discretised on a Cartesian grid according to a Marker-And-Cell (MAC) staggered finite-volume scheme and are sequentially solved using a fractional step algorithm [25]. The coupled mass-momentum problem is solved using a fractional step scheme through a pressure correction method. The time derivatives are approximated according to a first-order backward Euler scheme and the discrete convective operators are based on a hybrid centered-upwind scheme. The aforementioned choices ensure the unconditional stability of the time-stepping, so that no CFL constraint is required to set the time-step.

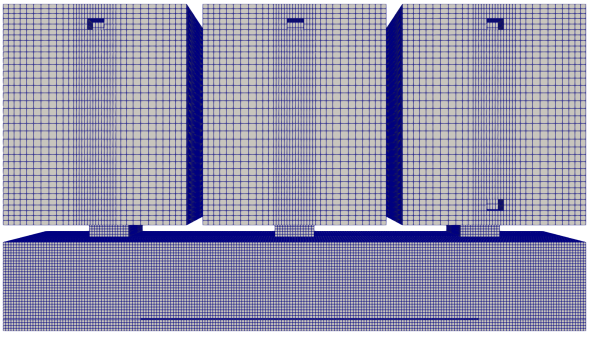

Figure 9: Mesh as viewed from above.

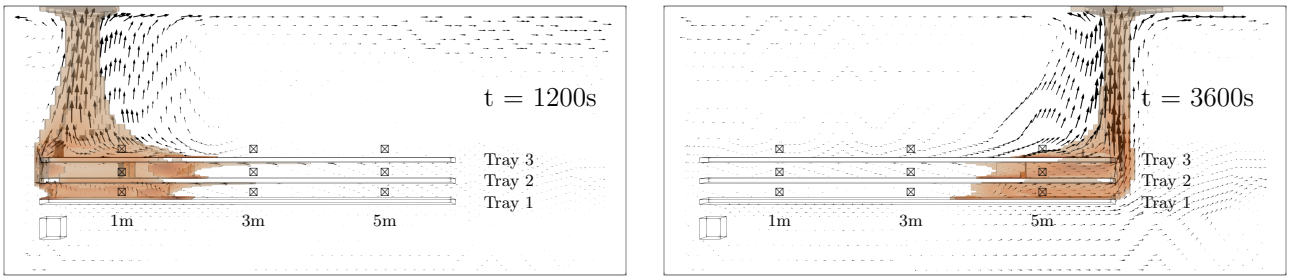

(a) FLASH-CAT simulation.

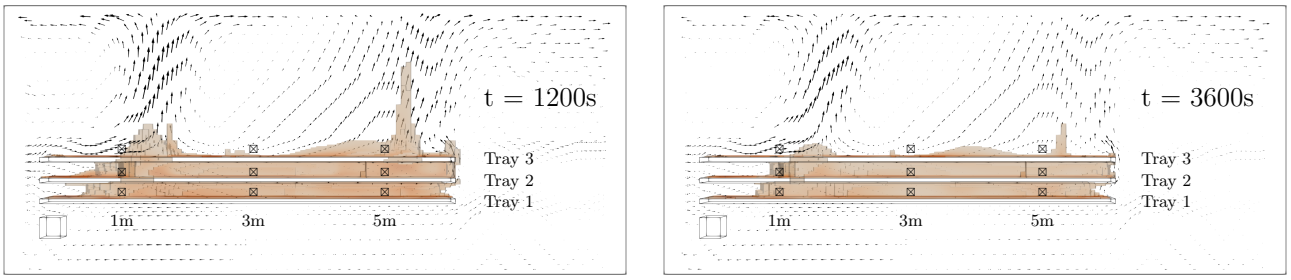

(b) Equivalent simulation.

Figure 10: Snapshots at 1200s and 3600s showing the plume location with superimposed velocity vector fields for the two simulation strategies. In this figure, the plume is defined from the reaction zone where the mixture fraction is greater than zero. The snapshot is taken from behind the cable trays with thermocouple locations (⊠) provided for Fig. 11.

Table 5
Meshing parameters. In this table, the characteristic length-scale of the cell is $\delta = (\delta x \delta y \delta z)^{\frac{1}{3}}$ or the cubic root of the cell volume.

	δ (m)			
No. cells	Fire	Corridor	Rooms	Overall
1050000	0.045	0.06	0.09	0.07

Simulations are then run with a time-step of 0.1s from the initial state, increasing to 0.5s once the flow was considered stable. The end of the simulation corresponds to 5500s, which is the experimental fire duration. Finally, once refined in the zones of interest, the mesh ensured a y^+ parameter everywhere inferior to 400 as recommended in the Best Practice Guidelines for fires of a similar type [26].

In order to provide a visualisation of the flow, snapshots over time of the two simulations are provided in Fig. 10 where the plume represents a reaction zone where the mixture fraction is greater than zero. The superimposed velocity vectors and plume locations show how the FLASH-CAT approach is capable of tracking the flame front throughout. Conversely, the somewhat constant reaction zone location of the equivalent simulation shows its limitations.

5. Results and discussion

In this section, comparisons are made between the experimental results, the simulation with a FLASH-CAT approach, and the second equivalent simulation without flame front propagation.

Taken from behind the cable trays, Fig. 10 shows the thermocouple locations with the origin as the beginning of the cable-trays. The direction of travel for the flame-front is then west to east. In Fig. 11 we plot the temperature profiles measured above the cable trays at the horizontal distances of 1m, 3m and 5m over time.

We begin with a discussion on the experimental temperature profiles. All profiles measured by the 6 thermocouples suggest the same distinct three phases beginning with a sharp rise, followed by a plateau and a steady fall. These three phases correspond to ignition, steady burning and extinction. The extended nature of the extinction phase, even after flames have subsided, is due partly to a smouldering effect which is not attempted to be captured in the present simulations. The extended nature of the extinction phase is mainly visible in Trays 1 and 2 as a result of falling debris from above increasing the effect of smouldering in the trays below. Further, a particularity is observed in Fig. 11 at 5m in Trays 1 and 2. Here, the thermocouples record highly elevated temperatures due to debris on the thermocouples.

The three phases are also visible in the FLASH-CAT simulations where propagation is clearly observed from west to east. Qualitatively, the FLASH-CAT simulation predicts reasonably well the peaks in temperatures above the cable trays. However, with respect to the profiles, the ignition

phase is delayed and the duration of the extinction phase is too short. The better predictions at 5m are due to the incorrect local MLRPUA profile adopted in the FLASH-CAT model. The latter assumes a more progressive increase of the local mass loss rate after ignition than that usually observed in cone calorimeter experiments. This results in a delayed ignition phase in the early stages of the propagation. The effect tends to decrease in the latter stages when a larger part of the trays is burning. Therefore, the MLRPUA profile used in the standard FLASH-CAT model, given as Fig. 5, can be improved in future studies with the use of material specific MLRPUA profiles. A further related improvement is in the ΔH_c of the fuel which includes the input from the burner. This contribution should be applied locally and for a limited duration. In future simulations, a multi-fuel approach will separate the propane mass injection from that of the equivalent fuel.

Qualitatively, the equivalent simulation predicts less well the peaks of the measured temperatures above the cable-trays as the flame front is not tracked. With respect to the profiles, they are in reasonable agreement with the experiment at a distance of 1m in Trays 1 and 2 where the long extinction phase exists.

For a more quantitative analysis the L^2 relative error norm can be calculated as,

$$\epsilon = \frac{\int_0^{\Delta T} \left(\phi_{\text{exp}}(t) - \phi_{\text{sim}}(t)\right)^2 dt}{\int_0^{\Delta T} \phi_{\text{exp}}(t)^2 dt} \tag{27}$$

with ϵ as the error and ϕ as the temperature, concentration or heat flux. The errors are provided for the FLASH-CAT (ε_f) and equivalent (ε_e) simulations in Fig. 11 and all figures hereupon. In this respect, the maximal error obtained with the FLASH-CAT approach ($\epsilon_f = 0.45$) is smaller than that obtained with the equivalent simulation ($\epsilon_e = 0.65$), which suggests a clear improvement. However, the average error over all thermocouples shown in Fig. 11 is 37% for both simulations as a result of the significant errors accumulated in the ignition phase for the flame front tracking method; an indication of where improvements can be made in future studies.

In Fig. 12 we plot the temperature profiles at three locations, provided in Fig. 8a as admission-side, centre and extraction-side of the corridor. Each profile then represents a temperature measurement at a height from the floor (see legend in Fig. 12). The experimental measurements show that the hot gases accumulate beneath the ceiling over time. Overall, the peaks in temperature are marginally better predicted by the FLASH-CAT approach. Quantitatively, however the average error over all thermocouples shown in Fig. 12 is very similar between the two simulation strategies.

In Figs. 13 and 14 we plot the oxygen and carbon dioxide concentration measurements in the corridor. The location of the gas analysers are provided in Fig. 8a. The oxygen concentration opposite the fire attains a minimum of $\sim$ 16% when HRR is at its peak around 3000s. Qualitatively, the FLASH-CAT approach predicts significantly better the peaks of the species concentrations. The average error over all sensors shown in Fig. 13 is again similar but concerning Fig. 14, the average error reduced by about 10% with the FLASH-CAT approach. The better predictions of product concentrations with the flame-front tracking method is an interesting observation for fires in long cable trays. Further error reductions will likely be observed if the aforementioned improvements to the MLRPUA profile in the FLASH-CAT approach are adopted.

Next, in Fig. 15, we plot the total heat flux measurements with the simulation predictions. As shown in Fig. 8b, the heat flux sensors were placed above the doorways in the corridor. The sensors measure convective plus radiative heat transfer. A maximum value is observed in the centre of the corridor, above the doorway to R2, with the lowest values measured above the doorway to R3. This is expected as, the fire source is closest to R2 and furthest away from R3 (see Fig. 8). The simulation adopting the FLASH-CAT approach over-predicts the maximum heat flux above the door to R2. The average error over all heat flux sensors shown in Fig. 15 is similar for both approaches with the main source of error in the FLASH-CAT simulation again appearing to be associated with the ignition phase.

Overall, the FLASH-CAT approach adopted here, better predicts the peaks in temperatures and concentrations but the overall profiles show similar average errors to simulations adopting the simpler equivalent approach. However, errors are likely to be reduced if a more physical description of the local degradation rate of the cable is used to define the MLRPUA profile opposed to the standard profile shown in Fig. 5. This will be the focus of future work.

6. Conclusions

In this paper, a PVC cable fire in horizontally stacked long cable-trays has been simulated numerically. The fire scenario is from the experimental CFP campaign carried out in the framework of the PRISME-3 OECD project. Implementation of a FLASH-CAT like approach in the CALIF^{3}S-Isis CFD code allowed for flame front tracking. The input parameters to the FLASH-CAT model were from experimental data and the flame front tracking method allowed for improved predictions of the experimental peaks in temperature, concentration and heat flux in the corridor. Further, the simulations carried out using the FLASH-CAT approach reduced the observed maximum error in the near-fire zone temperature predictions and in the predictions of species concentrations in the corridor. This latter finding highlights a potential benefit for flame-front tracking methods when simulating fires in long cable-trays.

It is noted, however, that the average error in the predictions of temperature, concentrations and heat fluxes were not reduced significantly with the use of a flame front tracking method. In future studies, fuel (cable) specific MLRPUA

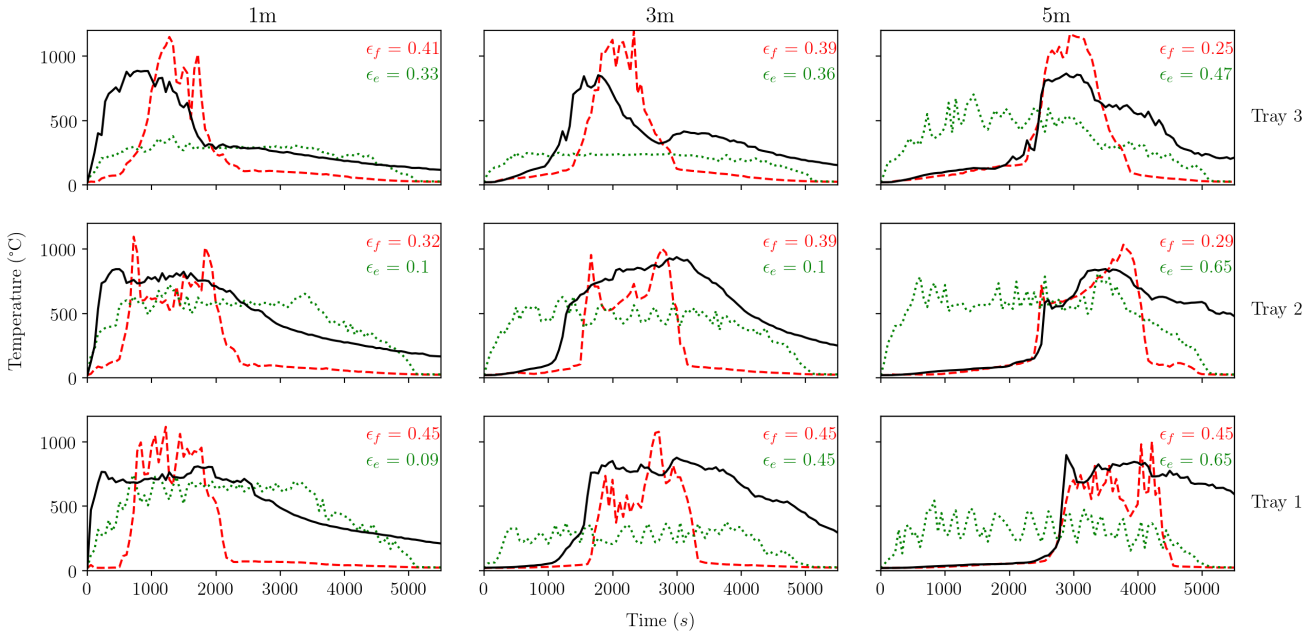

Figure 11: Temperature plots at three distances along the cable-trays. In this figure, temperatures are plotted for the experiment (▬▬), the simulation with the FLASH-CAT approach (▬ ▬ ▬) and the equivalent simulation without flame propagation (▪▪▪▪▪▪). The L^2 relative error norm, calculated using Eq. 27, is provided for the FLASH-CAT (ε_f) and equivalent (ε_e) simulation methods.

profiles should be implemented into the FLASH-CAT approach, allowing for more accurate injection profiles, especially in the ignition phase. Future efforts will also concentrate on utilising a multi-fuel approach so as to allow for the propane mass injection from the burner to be separated from the HRR of the equivalent fuel associated with FLASH-CAT.

Finally, this study has adopted a non-predictive FLASH-CAT approach where propagation is defined *a priori* from experimental data. Evidently, it would be preferable to predict flame propagation based on, for example, local temperature predictions and associated ignition criteria. This is an open area of research in which IRSN continues be to invested.

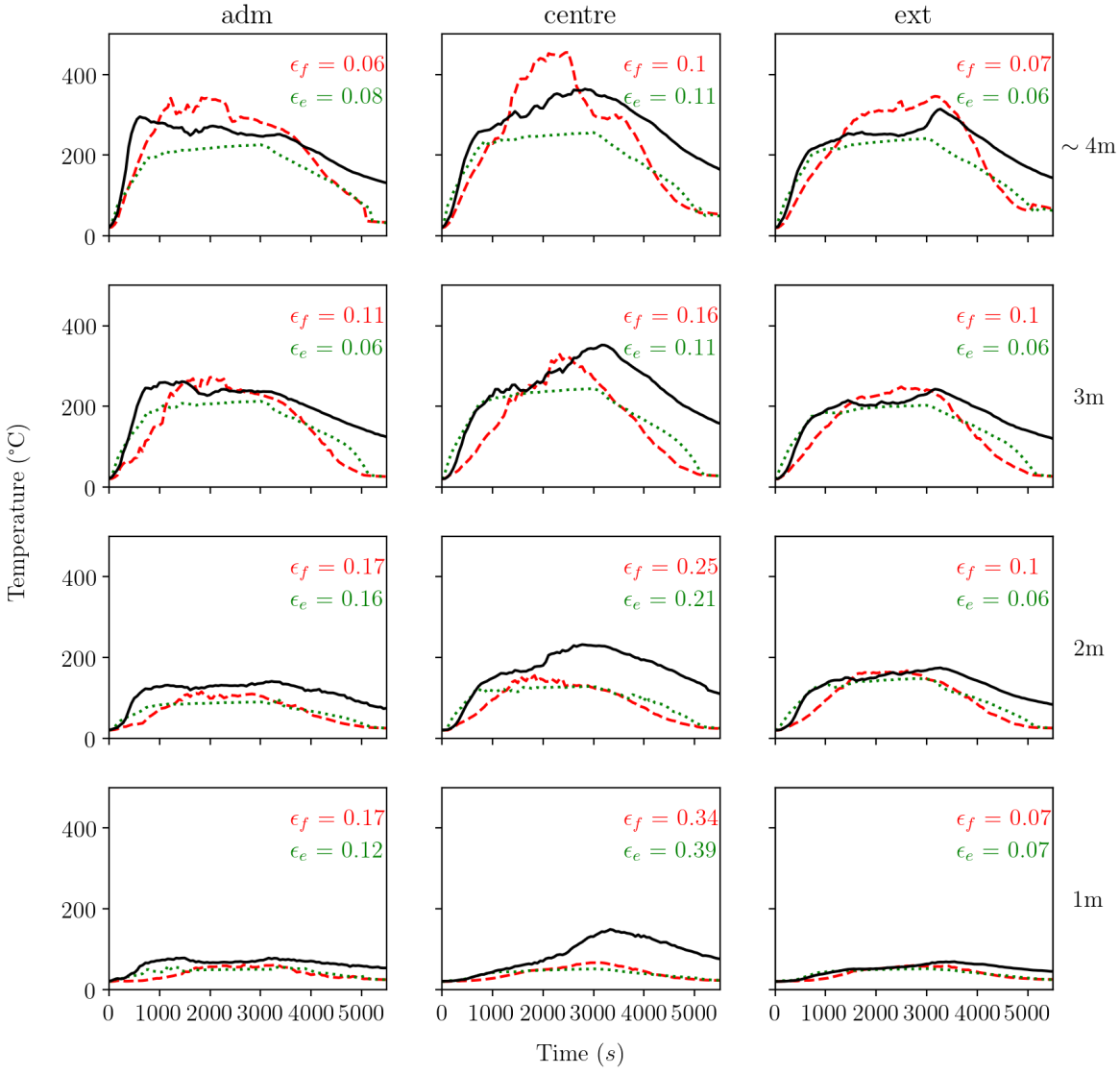

Figure 12: Temperature plots at three thermocouple tree locations in the corridor. In this figure, the legend is the same as in Fig. 11 and the location of the thermocouple trees are available in Fig. 8a. Results are presented at heights of 3.8, 3.0, 2.0 and 1.0 m from the ground.

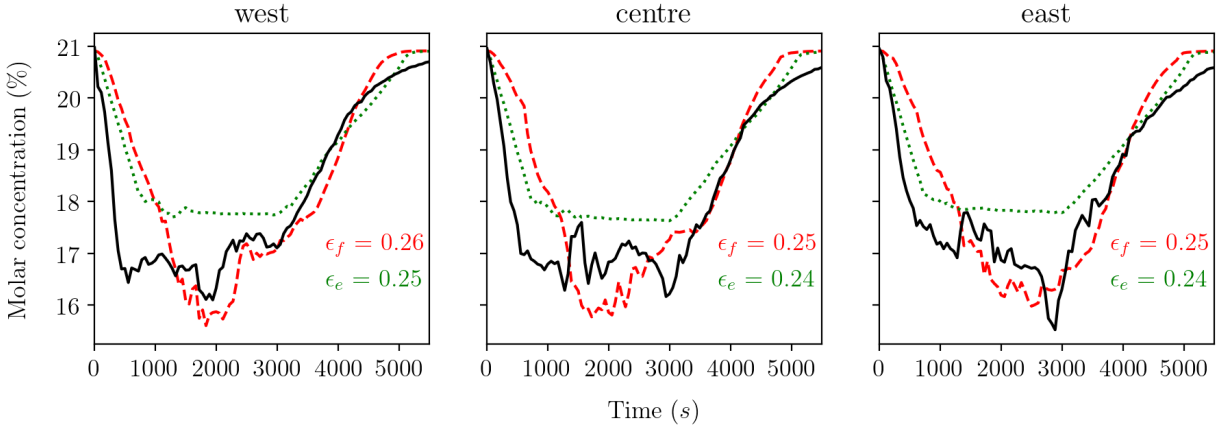

Figure 13: Oxygen concentration plots in the corridor at 3.3m from floor. In this figure, the legend is the same as in Fig. 11 and the location of the gas analysers are available in Fig. 8a.

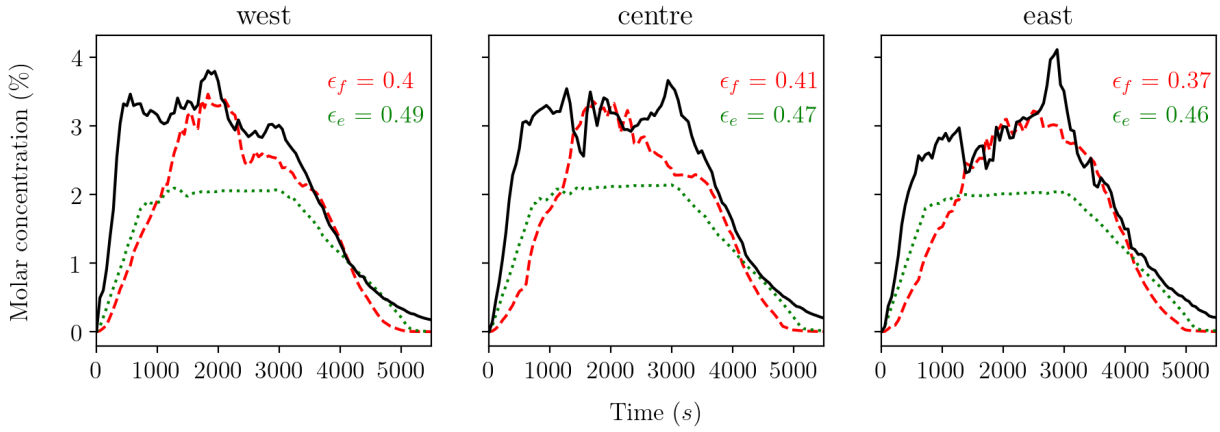

Figure 14: Carbon dioxide plots in the corridor measured in the corridor at 3.3m from floor. In this figure, the legend is the same as in Fig. 11 and the location of the gas analysers are available in Fig. 8a.

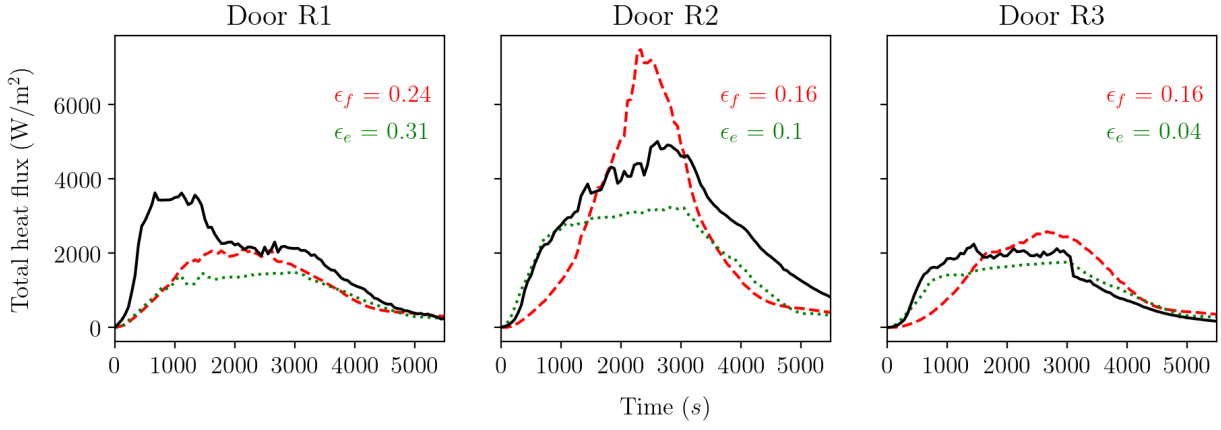

Figure 15: Heat flux plots measured above the doors in the corridor. In this figure, the legend is the same as in Fig. 11 and the location of the heat flux sensors are available in Fig. 8b.

References

[1] Organisation for Economic Co-operation and Development (OECD) Nuclear Energy Agency (NEA), Committee on the Safety of Nuclear Installations (CSNI), OECD/NEA FIRE Database Version. https://www.oecd-nea.org/jcms/pl_24954/fire-incidents-records-exchange-fire-project. Accessed: 2023-01-31.

[2] U.S. NRC, Cable Fire at Browns Ferry Nuclear Power Station, NRC Bulletin BL-75-04, U.S. Nuclear Regulatory Commission. https://www.nrc.gov/reading-rm/doc-collections/gen-comm/bulletins/1975/bl75004.html, 1975. Accessed: 2023-01-31.

[3] P.S. Sumitra. Categorization of cable flammability: intermediate-scale fire tests of cable tray installations Interim report. Technical Report EPRI-NP–1881, Factory Mutual Research Corp., 1982.

[4] M.M. Hirschler. Survey of fire testing of electrical cables. *Fire Mater.*, 16(3):107–118, 1992. doi: 10.1002/fam.810160302.

[5] S.J. Grayson, P. Van Hees, A.M. Green, H. Breulet, and U. Vercellotti. Assessing the fire performance of electric cables (FIPEC). *Fire Mater.*, 25(2):49–60, 2001. doi: 10.1002/fam.756.

[6] EPRI/NRC-RES. Fire PRA Methodology for Nuclear Power Facilities Volume 2: Detailed Methodology. EPRI TR-1011989 and NUREG/6850, Electric Power Research Institute (EPRI), Palo Alto, California, and U.S. Nuclear Regulatory Commission, Office of Nuclear Regulatory Research (RES), Rockville, Maryland, USA, 2005.

[7] K. McGrattan, A. Lock, N. Marsh, M. Nyden, S. Bareham, and M. Price. Cable Heat Release, Ignition, and Spread in Tray Installations During Fire (CHRISTIFIRE) Phase 1: Horizontal Trays. Technical Report NUREG/7010, National Institute of Standards and Technology, (NIST), 2012.

[8] W. Plumecocq, L. Audouin, and P. Zavaleta. Horizontal cable tray fire in a well-confined and mechanically ventilated enclosure using a two-zone model. *Fire Mater.*, 43(5):530–542, 2019. doi: 10.1002/fam.2698.

[9] J. Quintiere. *Surface Flame Spread*, chapter 2-12. Society of Fire Protection Engineers, Quincy, MA, 2002.

[10] P. Zavaleta, R. Hanouzet, and T. Beji. Improved assessment of fire spread over horizontal cable trays supported by video fire analysis. *Fire technol.*, 55(1):233–255, 2019. doi: 10.1007/s10694-018-0788-x.

[11] T. Beji and B. Merci. Numerical simulations of a full-scale cable tray fire using small-scale test data. *Fire Mater.*, 43(5):486–496, 2019. doi: 10.1002/fam.2687.

[12] S. Suard, C. Lapuerta, F. Babik, and L. Rigollet. Verification and validation of a cfd model for simulations of large-scale compartment fires. *Nucl. Eng. Des.*, 241(9):3645–3657, 2011. doi: 10.1016/j.nucengdes.2011.08.012.

[13] C. Lapuerta, S. Suard, F. Babik, and L. Rigollet. Validation process of ISIS CFD software for fire simulation. *Nucl. Eng. Des.*, 253:367–373, 2012. doi: 10.1016/j.nucengdes.2011.09.068.

[14] S. Suard, A. Nasr, S. Melis, J.-P. Garo, H. El-Rabii, L. Gay, L. Rigollet, and L. Audouin. Analytical approach for predicting effects of vitiated air on the mass loss rate of large pool fire in confined compartments. *Fire Saf. Sci.*, 10:1513–1524, 2011. doi: 10.3801/IAFSS.FSS.10-1513.

[15] P. Becerra Barrios, H. Pretrel, S. Vaux, and O. Vauquelin. Flow behaviour of the exchange flow through a ceiling vent in natural convection: A numerical approach using CALIF3S-ISIS CFD software. *J. Phys. Conf. Ser.*, 1107(4):042019, 2018. doi: 10.1088/1742-6596/1107/4/042019.

[16] S. Vaux, H. Prétrel, and L. Audouin. Experimental and numerical study of water spray system for a fire event in a confined and mechanically ventilated compartment. *Fire Mater.*, 43(5):579–590, 2019. doi: 10.1002/fam.2719.

[17] M. Siemon, O. Riese, B. Forell, D. Krönung, and W. Klein-Heßling. Experimental and numerical analysis of the influence of cable tray arrangements on the resulting mass loss rate and fire spreading. *Fire Mater.*, 43(5):497–513, 2019. doi: 10.1002/fam.2689.

[18] J. Seguillon and H. Pretrel. Experimental study of large-scale long cable tray fire in a confined and mechanically ventilated environment. *Fire Saf. J. VSI: PRISME3 Project*, In press.

[19] S. Bascou, P. Zavaleta, and F. Babik. Cable tray fire tests simulations in open atmosphere and in confined and mechanically ventilated compartments with the CALIF^{3}S-Isis CFD software. *Fire Mater.*, 43(5):448–465, 2019. doi: 10.1002/fam.2680.

[20] A. Favre. Turbulence: Space-time statistical properties and behavior in supersonic flows. *Phys. Fluids*, 26(10):2851–2863, 1983. doi: 10.1063/1.864049.

[21] G. D. Raithby and E. H. Chui. A Finite-Volume Method for Predicting a Radiant Heat Transfer in Enclosures With Participating Media. *J. Heat Transfer*, 112(2):415–423, 05 1990. ISSN 0022-1481. doi: 10.1115/1.2910394.

[22] T. F. Smith, Z. F. Shen, and J. N. Friedman. Evaluation of coefficients for the weighted sum of gray gases model. *J. Heat Transfer (Trans. of the ASME)*, 104:602–608, 1982. doi: 10.1115/1.3245174.

[23] R. Siegel and J. R. Howell. *Thermal Radiation Heat Transfer*. Hemisphere Publishing Corporation, Washington D.C., 1992.

[24] B. F. Magnussen and B. H. Hjertager. On mathematical modeling of turbulent combustion with special emphasis on soot formation and combustion. *Symp. (Int.) Combust.*, 16(1):719–729, 1977. doi: 10.1016/S0082-0784(77)80366-4.

[25] F. Babik, T. Gallouet, J.-C. Latché, S. Suard, and D. Vola. *On two fractional step finite volume and finite element schemes for reactive low Mach number flows*, pages 505–514. Wiley-ISTE, Quincy, MA, 2005.

[26] G. Cox and S. Kumar. *Modeling Enclosure Fires Using CFD*, chapter 3-8. Society of Fire Protection Engineers, Quincy, MA, 2002.